

Research Paper

Cite this article: Gumma MK *et al.* (2020). Assessing potential locations for flood-based farming using satellite imagery: a case study of Afar region, Ethiopia. *Renewable Agriculture and Food Systems* 1–15. <https://doi.org/10.1017/S1742170519000516>

Received: 28 April 2019

Revised: 15 November 2019

Accepted: 21 November 2019



Key words:

Afar; Ethiopia; flooded areas; Google Earth Engine; landsat-8; LULC; MODIS; sentinel-1

Author for correspondence:

Murali Krishna Gumma,
E-mail: m.gumma@cgiar.org,
gummamk@gmail.com

Assessing potential locations for flood-based farming using satellite imagery: a case study of Afar region, Ethiopia

Murali Krishna Gumma^{1,2} , Tilahun Amede¹, Mezegebu Getnet¹,
Bhavani Pinjarla², Pranay Panjala², Gizachew Legesse¹, Gebeyaw Tilahun³,
Elisabeth Van den Akker⁴, Wolf Berdel⁴, Christina Keller⁴, Moses Siambi¹
and Anthony M. Whitbread⁵ 

¹International Crops Research Institute for the Semi-Arid Tropics (ICRISAT), Addis Ababa, Ethiopia; ²RS/GIS lab, SACS, ISD, International Crops Research Institute for the Semi-Arid Tropics (ICRISAT), Patancheru, Telangana, India; ³Woldya University, Woldya, Ethiopia; ⁴GIZ-Ethiopia, Addis Ababa, Ethiopia and ⁵Innovations Systems in the Drylands, International Crops Research Institute for the Semi-Arid Tropics (ICRISAT), Patancheru, Telangana, India

Abstract

The dry lowlands of Ethiopia are seasonally affected by long periods of low rainfall and, coinciding with rainfall in the Amhara highlands, flood waters which flow onto the lowlands resulting in damage to landscapes and settlements. In an attempt to convert water from storm generated floods into productive use, this study proposes a methodology using remote sensing data and geographical information system tools to identify potential sites where flood spreading weirs may be installed and farming systems developed which produce food and fodder for poor rural communities. First, land use land cover maps for the study area were developed using Landsat-8 and MODIS temporal data. Sentinel-1 data at 10 and 20 m resolution on a 12-day basis were then used to determine flood prone areas. Slope and drainage maps were derived from Shuttle RADAR Topography Mission Digital Elevation Model at 90 m spatial resolution. Accuracy assessment using ground survey data showed that overall accuracies (correctness) of the land use/land cover classes were 86% with kappa 0.82. Coinciding with rainfall in the uplands, March and April are the months with flood events in the short growing season (*belg*) and June, July and August have flood events during the major (*meher*) season. In the Afar region, there is potentially >0.55 m ha land available for development using seasonal flood waters from *belg* or *meher* seasons. During the 4 years of monitoring (2015–2018), a minimum of 142,000 and 172,000 ha of land were flooded in the *belg* and *meher* seasons, respectively. The dominant flooded areas were found in slope classes of <2% with spatial coverage varying across the districts. We concluded that Afar has a huge potential for flood-based technology implementation and recommend further investigation into the investments needed to support new socio-economic opportunities and implications for the local agro-pastoral communities.

Introduction

A rising global population has increased the pressures on natural resources for agriculture, livestock and livelihood needs. Concomitantly, there is a decline in productive areas in sub-Saharan Africa partly caused by flash floods, droughts, land degradation and associated declines in soil fertility (Amede *et al.*, 2004). The low lying regions of Ethiopia, largely located in the Great Rift Valley, are prone to extreme events of recurrent drought and flood (Gummadi *et al.*, 2017). Land degradation is also a common problem in the region (Miheretu and Yimer, 2018), with more than 1.5 billion tonnes of topsoil from higher elevated areas washed away by heavy rains (Tamene and Vlek, 2008; Miheretu and Yimer, 2018).

In Ethiopia, the highlands, which occupy 44% of total geographical areas, have been under cultivation for centuries and are severely affected by soil erosion (Hurni, 1988) and deforestation (McCann, 1997). The highlands are the source of flash floods and sediment loads to the neighboring downstream lowlands. In the decades past, flood waters were reported to have spread across the low-lying grazing lands (Hailu *et al.*, 2018), benefiting the rangelands which supported the livelihoods of (agro) pastoralists. With large numbers of livestock and year-round grazings, the (agro) pastoral landscapes of Afar have degraded and the flood channels have become deep gullies (Van Steenberg *et al.*, 2011) with less chance for the waters to spread and irrigate natural pastures.

Pilot studies in the degraded Rift Valley areas of Ethiopia demonstrated that the effects of strong runoff and sporadic flash floods could be reversed by a holistic approach using water spreading weirs (WSW) (Elisabeth *et al.*, 2015). WSW are low retention walls commonly built in the foot slopes of mountainous landscapes, designed to regulate seasonal floodwaters,

© The Author(s), 2020. Published by Cambridge University Press. This is an Open Access article, distributed under the terms of the Creative Commons Attribution licence (<http://creativecommons.org/licenses/by/4.0/>), which permits unrestricted re-use, distribution, and reproduction in any medium, provided the original work is properly cited.

reduce runoff and minimize erosion (Haile and Fetene, 2012). The weirs could modify waterways, catchments and farms at scale. Improved management of land and water resources for the sustainable development through improved management of spate irrigation has been reported earlier (Gumma *et al.*, 2011). Several studies have proven that successful management and use of spate irrigation and broader natural resources management would require integrated approaches considering social and biophysical processes (Moore *et al.*, 1991; Vittala *et al.*, 2008; Iqbal and Sajjad, 2014; Panwar and Singh, 2014) and appropriate use of tools and methods.

Remote sensing is one of the low cost but effective tools for monitoring natural resources and flooded areas on timely basis. A wide range of satellites is capturing information at various spatial, spectral, temporal and radiometric resolutions. Near real time satellite imagery helps in identifying droughts and floods for quick decisions (Gumma *et al.*, 2017). Numerous studies have been conducted on monitoring croplands and natural resources using remote sensing and geographical information systems supported by secondary information (Rao *et al.*, 2001; Gumma *et al.*, 2009, 2015, 2018b; Qiu *et al.*, 2013). Several studies mapped water bodies, flooded areas and soil moisture regimes using multiple data sets including MODIS, Landsat and sentinel (Feyisa *et al.*, 2014; Gumma *et al.*, 2015; Qiu *et al.*, 2015). Temporal satellite imagery and spectral analysis were successfully used in monitoring croplands and flooded areas in various studies (Gumma *et al.*, 2014; Dong *et al.*, 2015; Gumma *et al.*, 2019), including at watershed and higher scales (Khan *et al.*, 2001; Gumma *et al.*, 2016). For instance, Sentinel-1 is most widely used to map soil moisture and floods during rainy season (Paloscia *et al.*, 2013; Pierdicca *et al.*, 2014; Schlaffer *et al.*, 2015) including for assessment of flood damage.

Flood events occur where the overflow of water submerges land due to high rainfall events, an overflow of water from a water body, or in the case of the Afar region, from seasonal flows from the uplands (Flick *et al.*, 2012). Synthetic Aperture Radar (SAR) data has been found to effective for near real-time flood monitoring because of its ability to penetrate cloud cover which renders multispectral satellite data useless in the event of flood due to heavy rainfall. It can thus be used to map inundated areas (standing water) after heavy rainfall and to assess the flood damage, as standing water appears dark in SAR images due to specular reflection. The rough surface of fast flowing water, or that caused by rain or wind, cannot be mapped by SAR data because the roughness increases radar backscatter, giving a bright signature on the SAR image (Alsdorf *et al.*, 2007; Jung *et al.*, 2010). A change detection algorithm, mapping the difference between the images before and after flooding, has been shown to bring out the inundated areas effectively (Giustarini *et al.*, 2013; Schlaffer *et al.*, 2015).

Given the fact that the rift valley regions of Ethiopia are remote and data scarce, the objective of this paper is to demonstrate a method to assess and map flood prone areas to support flood-based management technologies and practices for converting flash floods to a productive use and supporting livelihoods by enhancing crop and fodder productivity across the Afar region. The paper also intends to provide quantitative estimates of flooded areas across districts of Afar that could lead to prioritization of actions and investment.

Study area

The study was carried out in the Afar region which is a sub-set of Danakil and Awash River basins of Ethiopia. The region is

structured into five administrative zones and 29 districts. The altitude ranges from the lowest point of 116 m below sea level to about 2063 m above sea level (Fig. 1). As one of the hottest places on Earth, temperatures reaching 50°C are not uncommon. The annual average rainfall ranges from <100 mm in the lowland areas to >500 mm in the surrounding highlands.

The region is found within the Danakil and Awash River Basin, which is located between 7°53'N and 12°N latitudes and 37°57'E and 43°25'E of longitudes (Taddese *et al.*, 2003), covering a total land area of 110,000 km². The largest part of the Awash River Basin is located in the arid lowlands of the Afar Region in the northeastern part of Ethiopia which extends from semi-desert lowlands to cold high mountainous zones with extreme ranges of temperature and rainfall. There are three seasons in the Awash River Basin namely *meher* (rainy season/June–September), *Bega* (dry season/October–January) and *belg* (small rainy season/February–May). The region is hydrologically connected to the highlands of Oromia, Amhara and Tigray regional states from which the lowland of Afar receives floods occurring during the *belg* and *meher* seasons.

Data and methods

Satellite imagery and data preparation

MODIS NDVI 250 m

MODIS Terra Vegetation Indices 16-Day L3 Global 250 m SIN Grid V005 (MOD13Q1 product) imagery were used, which are freely available from the Land Processes Distributed Active Archive Center (https://lpdaac.usgs.gov/lpdaac/get_data/data_pool). MOD13Q1 16-day composite, four-band data for all 23 composite dates during January–December, 2017 were used in this analysis. Bands and vegetation indices contained in the MOD13Q1 product include blue, red and near infrared (NIR) and mid-infrared bands and normalized differentiation vegetation (NDVI) index (NDVI generated using NIR and red bands). The product is already atmospheric corrected and cloud contamination generated using 16-days maximum composite NDVI. Table 1 provides the data used in the study and description.

Landsat-8 imagery

Landsat-8 images extracted from USGS Earth explorer (<https://earthexplorer.usgs.gov/>). In this study, we have used 11 Landsat 8 tiles (February 2017 and November 2017) which were captured in *belg* and *meher* seasons (Table 1). Image preprocessing start with image normalization, which means converting sensor captured digital number (DN) values to the reflectance.

Image normalization: The following equation is used to convert DN values to top of atmosphere (TOA) reflectance for OLI data

$$\lambda' = M_p Q_{cal} + A_p \quad (1)$$

where λ' is the TOA planetary reflectance (without correction of solar angle), M_p is the Band specific multiplicative rescaling factor from the metadata, A_p is the band specific additive rescaling factor from the metadata and Q_{cal} is the quantized and calibrated standard product pixel values (DN).

TOA reflectance with correction for the sun angle is then:

$$\lambda = \frac{\lambda'}{\sin(\theta_{SE})} \quad (2)$$

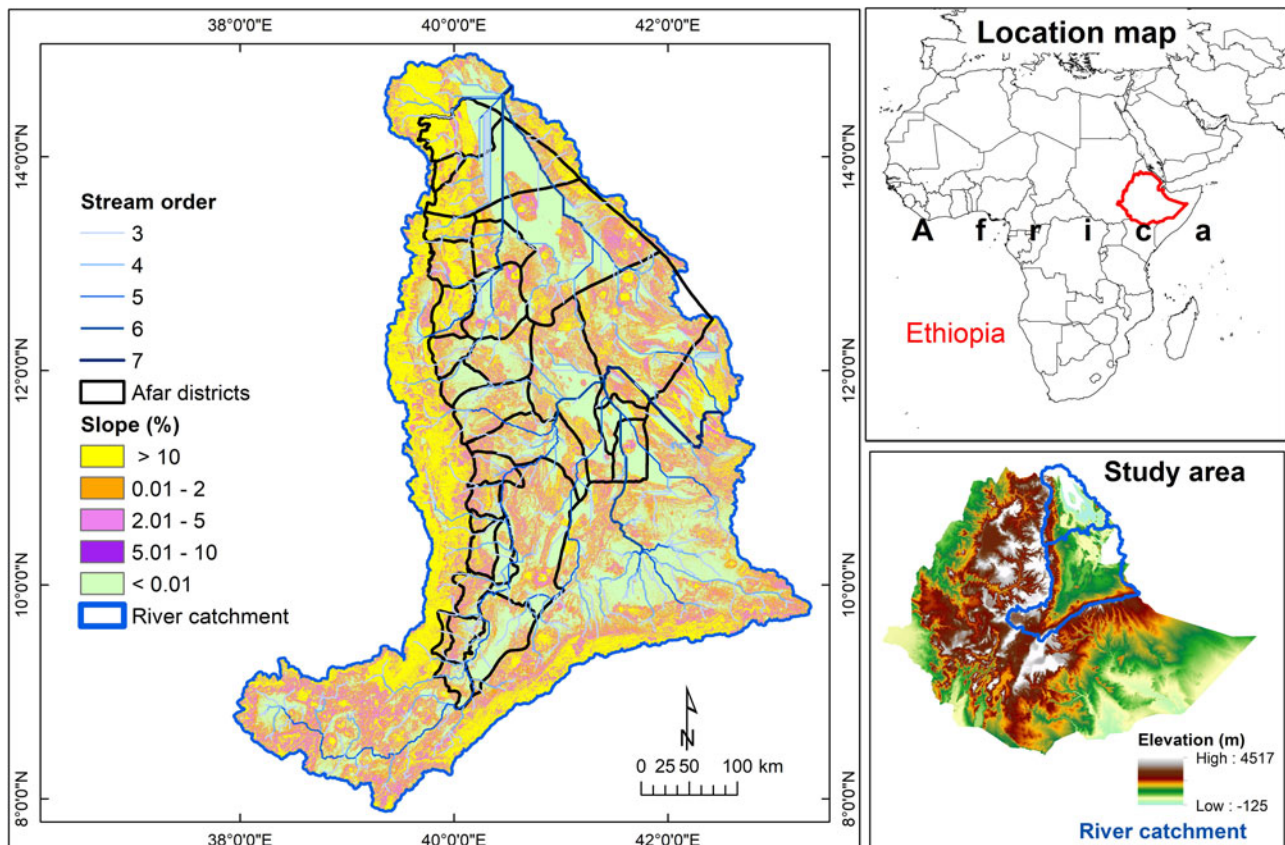


Fig. 1. Location map of the Afar region with major rivers and climate zones.

where λ is the TOA planetary reflectance, λ' is the TOA planetary reflectance (without correction of solar angle) and θ_{SE} is the local sun elevation angle provided in the metadata (SUN_ELEVATION).

Sentinel-1 data

The Sentinel-1 mission provides data from a dual-polarization C-band Synthetic Aperture Radar (SAR) instrument. This collection includes the S1 ground range detected (GRD) scenes, processed using the Sentinel-1 Toolbox to generate a calibrated, ortho-corrected product. The collection is updated weekly. The GRD scenes either of the three resolutions (10, 25 or 40 m). It consists of combinations of four bands i.e., single band VV or HH, and dual band VV + VH and HH + HV: 1. VV: single co-polarization, vertical transmit/vertical receive 2. HH: single co-polarization, horizontal transmit/horizontal receive 3. VV + VH: dual-band cross-polarization, vertical transmit/horizontal receive 4. HH + HV: dual-band cross-polarization, horizontal transmit/vertical receive (Sentinel-1 User Handbook, 2013, ESA, 2014). The data is freely available from Copernicus Open Access Hub the open hub site or it can be accessed from cloud computing platform Google Earth Engine.

In the study in order to assess the flooded areas, the freely available Sentinel-1 GRD, single band VV polarized data during peak flood periods of the Ethiopia region i.e., February–September 2017 downloaded from open access hub site (<https://scihub.copernicus.eu/dhus/>).

SRTM DEM data

The Shuttle Radar Topography Mission (SRTM) – a mission of NASA provides information regarding surface topography for

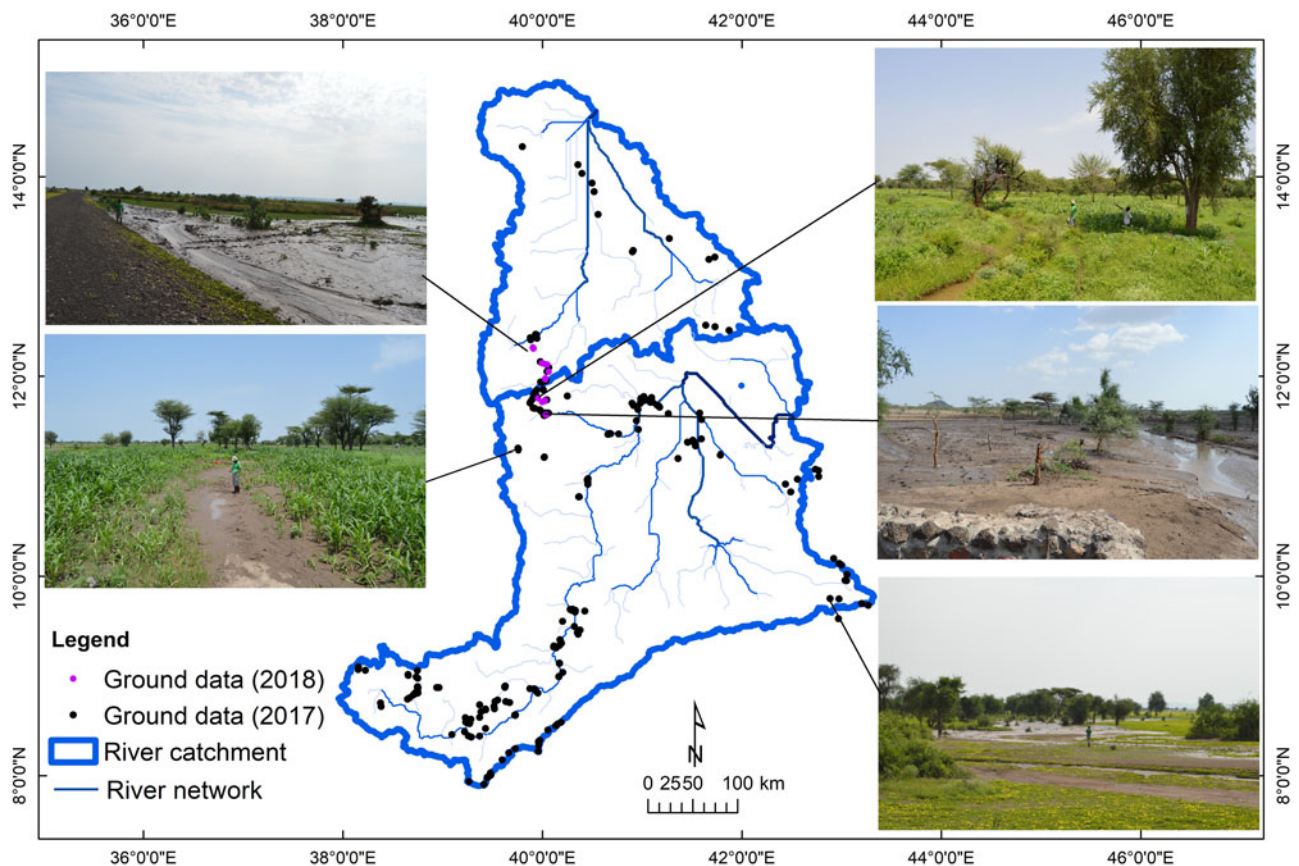
better understanding of geospatial features of Earth which is obtained from elevation data at 90 m spatial resolution on a near-global scale to generate the most complete high resolution digital topographic database of the Earth (SRTM technical guide). SRTM data can be downloaded from USGS Earth Explorer at 30 m (1-Arc Second) and 90 m resolutions. In this study we used DEM for extraction of a slope.

Ground survey data

A ground survey was conducted in 2 different years, the first visit was done in August 2017 and the second one was during August 2018 for the *meher* season. The survey was conducted as training and validation, for both classifying land use/land cover (LULC) and assessing the accuracy map. Altogether 316 locations (65 locations in 2018 and 251 locations in 2017) covering major land use/land cover areas in entire river catchment were recorded. Each location, data were collected from 90×90 m plots and consisted of GPS locations, land use categories, land cover percentages, cropping pattern during different seasons (through farmer interviews), crop types and watering method (irrigated, rainfed) along with other LULC areas. Samples were obtained within large contiguous areas of a particular LULC. Locations were chosen based on the knowledge of field staff and agriculture officers to ensure that the crops were grown during the *belg* season during the survey. Overall, 316 spatially well-distributed data points (Fig. 2) were collected; of these, 68 data points were used for identification and labeling class names while an additional 248 data points were used for accuracy assessment.

Table 1. Data used for the present study and characteristics of satellite sensor data used in the study

Imagery	Bands #	Band width nm ³ /range	Potential application
Landsat-8 data sets			
	Band 2 – Blue	0.450–0.515	Water bodies and also capable of differentiating soil and rock surfaces from vegetation
	Band 3 – Green	0.525–0.600	Emphasizes peak vegetation, which is useful for assessing plant vigor
	Band 4 – Red	0.630–0.680	Sensitive to strong chlorophyll absorption region and strong reflectance region for most soils.
	Band 5 – NIR	0.845–0.885	Operates in the best spectral region to distinguish vegetation varieties and conditions
	Band 6 – SWIR1	1.560–1.660	Discriminates moisture content of soil and vegetation; penetrates thin clouds
	Band 7 – SWIR2	2.100–2.300	Improved moisture content of soil and vegetation and thin cloud penetration
	Band 10 – TIR1	10.6–11.2	Thermal mapping and estimated soil moisture
	Band 11 – TIR2	11.5–12.5	Improved thermal mapping and estimated soil moisture
SRTM 90 m	meters		Extraction of slope
Sentinel-1		SAR	Flood mapping
MOD13Q1 – 250 m 16 days NDVI	NDVI	–1 to +1	Vegetation conditions

**Fig. 2.** Ground survey data locations in Afar regions during *meher* season.

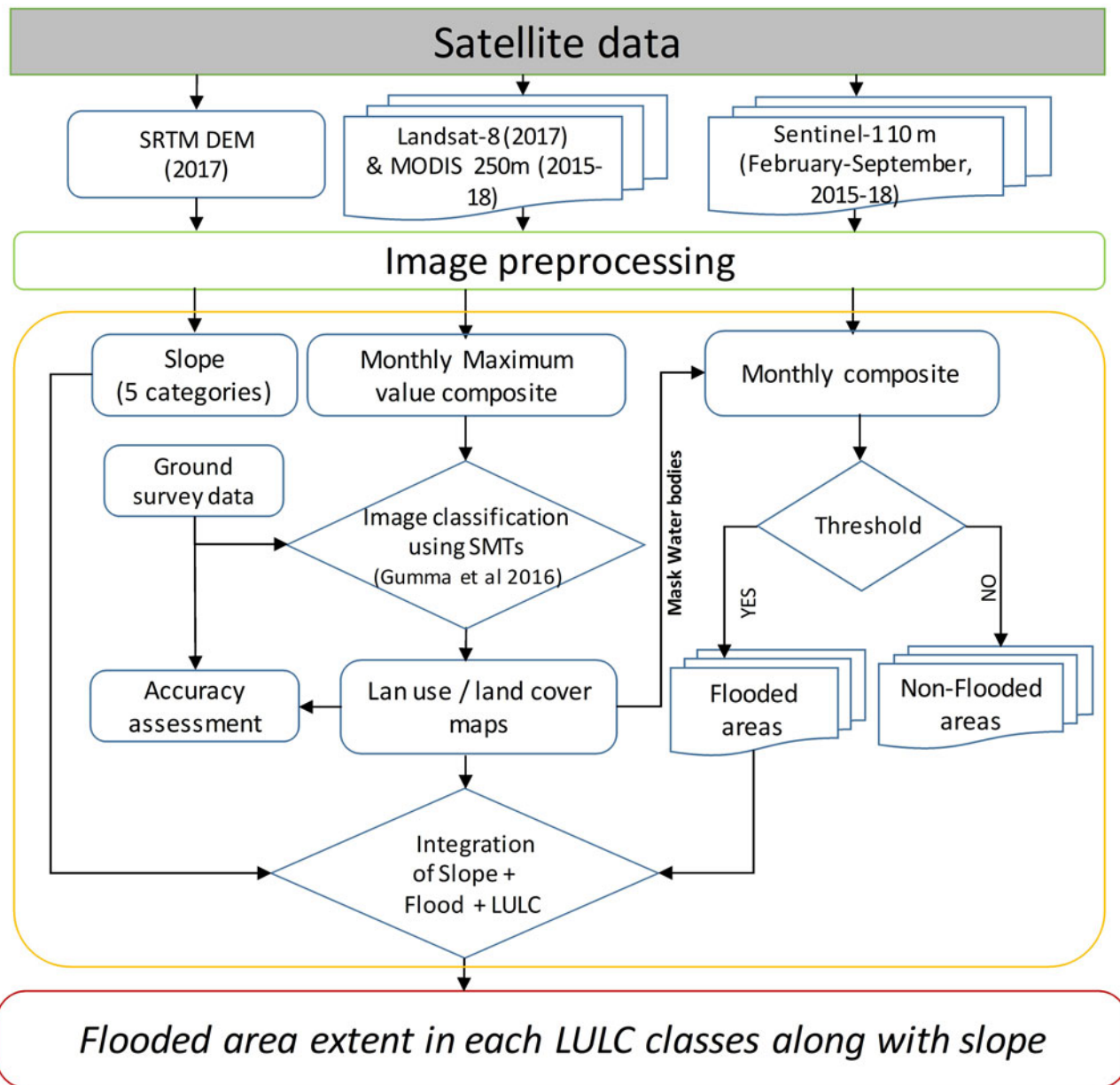


Fig. 3. Overview of the methodology for assessing flood prone areas using integrated remote sensing techniques.

The methodology for the identification and mapping of flood prone areas and areas targeting of new technologies is shown in Figure 3 and is described in the following sections. We have started the process with multi sensor image preprocessing

Land use/land cover classification

A time series of MODIS 16-day composite vegetation index images at 250 m resolution were obtained for the period of 01 January 2017 to 31 December 2017 (MOD13Q1 data product). The 16-day composite images in the MOD13Q1 dataset are available in the public domain and are pre-calibrated (<http://modis-sr.1tdri.org/html>). The large scene size and daily overpass rate of MODIS makes it attractive for mapping large crop areas, and NDVI derived from MODIS has high fidelity with biophysical parameters (Gumma *et al.*, 2018a). The 16-day NDVI images

were stacked into a 23-band file for each crop year (two images per month). The monthly maximum value composites were created using 16-day NDVI MODIS data to minimize cloud effects.

Unsupervised classification as described by Cihlar *et al.* (1998) was used to generate initial classes. The unsupervised ISOCCLASS cluster algorithm (ISODATA in ERDAS Imagine 2014TM) run on the NDVI-MVC generated an initial 40 classes, with a maximum of 100 iterations and convergence threshold of 0.99. Though ground survey data was available at the time of image classification, unsupervised classification was used in order to capture the full range of NDVI over a large area. The use of unsupervised techniques is recommended for large areas that cover a wide and unknown range of vegetation types, (Biggs *et al.*, 2006). Based on the above methodology, we classified LULC for the entire study area.

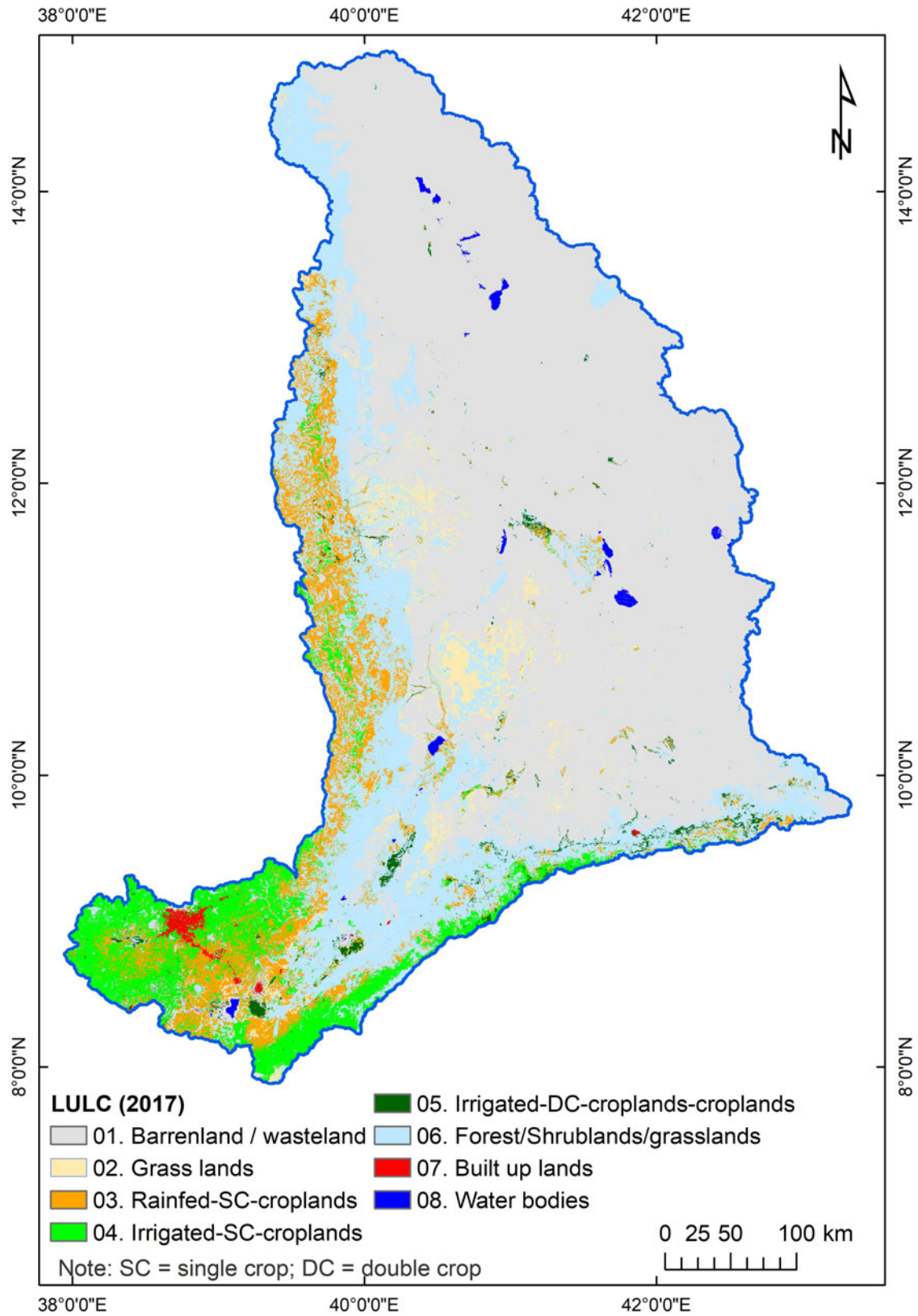


Fig. 4. Spatial distribution of LULC (derived from 2017 MODIS composite) (Note: SC, single crop; SW, surface water; DC, double crop).

Table 2. Area coverage and relative proportion of the eight LULC classes for the year 2017

LULC	Area in '000 ha	%
01. Barren land/wasteland	11,501	58
02. Grass lands	644	3
03. Rainfed-SC-croplands	1493	8
04. Irrigated-SC-croplands	1263	6
05. Irrigated-DC-croplands-croplands	176	1
06. Forest/shrub lands/grasslands	4531	23
07. Built up lands	79	0
08. Water bodies	82	0

SAR processing

Google Earth Engine’s collection of Sentinel-1 data contains all the GRD images from 03rd October 2014. These are the Level-1 scenes processed to backscatter coefficients (σ_0) in decibels (dB) (Sentinel-1 User Handbook, 2013, ESA, 2014). The steps involved in pre-processing of the Sentinel-1 images in order to obtain the Level-1 backscatter images are: (1) application of orbit file; (2) removal of GRD border noise and invalid data on the scene edges; (3) thermal noise removal to remove additive noise in sub-swaths; (4) radiometric calibration to compute the backscatter intensity and (5) terrain correction to compute σ_0 on the basis of Digital Elevation Model (DEM). VV polarized images were considered as advantageous for flood mapping when using Sentinel-1 data (Gumma *et al.*, 2015; Twele *et al.*, 2016).

Monthly composite images were computed from the pre-processed images to carry the monthly pattern of flooding during 2017 (eight images in a year). Masking of the non-water bodies from the sentinel 1 images was done using the above prepared LULC (2016–2017) as the reference map.

A well-known fact is that water bodies have low backscattering radar signals due to flat and smooth surface. A simple thresholding technique applied on the radar backscatter image, with the threshold values based on a visual inspection and expert knowledge, would effectively map the submerged areas, when these areas are open and considerably larger in size than the spatial resolution of the Sentinel-1 images. Finally, flooded areas/water bodies were mapped and non-flooded areas were masked. These steps were repeated for 3 years, 2015 to 2018, with eight independent images per year.

Submergence of flooded area

We have integrated the slope and flood files to generate the submergence of area in each of the slope category. Finally, the LULC map was integrated with the submergence (flooded) area while the extent of LULC was extracted for each class areas affected with flood. Figure 3 illustrates the overall methodology of assessing the submergence (flooded) area extent in each LULC class. A land-water threshold was manually applied to classify the images into two classes: land and water.

Assessing flood prone areas

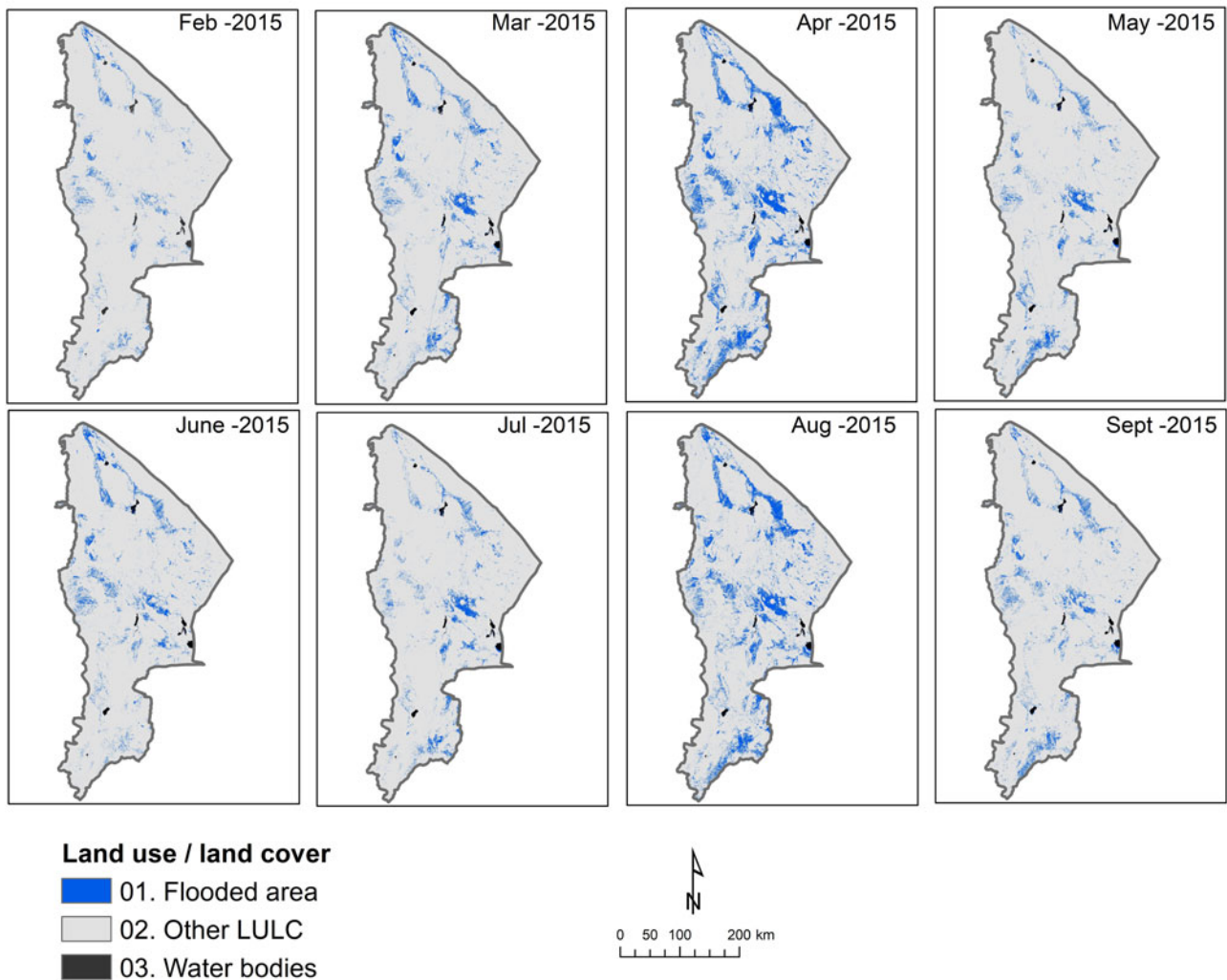
After monthly mapping of flood for the *belg* and *meher* seasons, we quantified flood frequency during 4 years (2015–2018)

Table 3. Accuracy assessment of Landsat derived LULC classes through error matrix using ground data

Classified data	Ground survey data								Row total	Classified total	Number of correct	Producer accuracy (%)	User accuracy (%)	κ
	CL_1	CL_2	CL_3	CL_4	CL_5	CL_6	CL_7	CL_8						
CL_1	49	0	0	0	1	0	1	2	53	53	49	94	92	0.9
CL_2	0	12	0	0	0	0	0	0	12	12	12	92	100	1.0
CL_3	0	0	16	0	1	0	2	0	19	19	16	73	84	0.8
CL_4	0	0	0	10	1	0	2	0	13	13	10	100	77	0.8
CL_5	0	0	0	0	27	0	1	0	28	28	27	77	96	1.0
CL_6	3	1	4	0	2	69	9	0	88	88	69	100	78	0.7
CL_7	0	0	2	0	3	0	11	0	16	16	11	42	69	0.7
CL_8	0	0	0	0	0	0	0	8	8	8	8	80	100	1.0
Reference totals	52	13	22	10	35	69	26	10	248	248	213			

Table 4. Flooded area extent in each LULC classes along with slope

LULC	Area in ha			
	01. Flood & <2% slope	02. Flood & 2–3% slope	03. Flood & >3% slope	04. Other
01. Barren land/wasteland	2,526,480	54,087	120,681	8,799,530
02. Grass lands	136,510	2431	3325	502,224
03. Rainfed-SC-croplands	31,670	5025	38,272	1,418,490
04. Irrigated-SC-croplands	9628	7870	26,154	1,219,800
05. Irrigated-DC-croplands-croplands	9005	236	2483	163,899
06. Forest/Shrub lands/grasslands	232,097	17,144	103,998	4,177,350
07. Built up lands	717	228	231	78,255
08. Water bodies	73,483	394	83	8517

**Fig. 5a.** Spatiotemporal distribution of floods in the Afar administrative region during 2015.

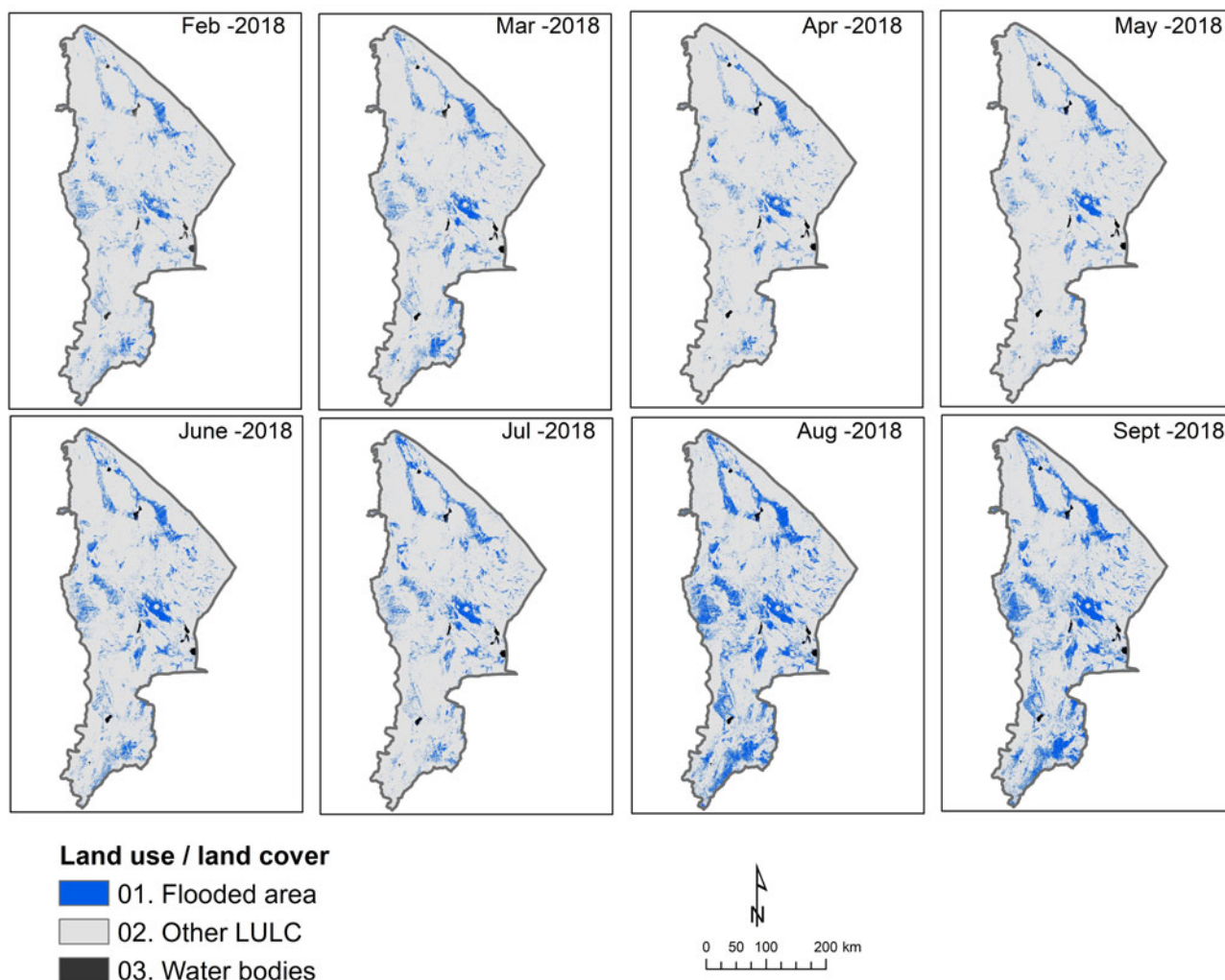


Fig. 5b. Spatiotemporal distribution of floods in the Afar administrative region during 2018.

Table 5. Temporal flooded areas across the Afar region

Month	Area in Ha			
	Year 2015	Year 2016	Year 2017	Year 2018
February	291,721	693,188	744,735	656,521
March	550,027	555,870	738,974	731,490
April	1,208,610	689,005	726,302	553,019
May	467,763	635,207	555,318	569,904
June	518,008	416,088	517,985	950,847
July	443,004	815,498	719,559	887,241
August	1,134,080	1,545,220	1,323,870	1,660,330
September	498,923	639,489	446,365	1,592,400

considering only flood class. The ERDAS modeler was used to quantify the frequency of flood from 2015 to 2018, considering pixel wise flood. Equation (3) was used to assess flood frequency from 2015 to 2018.

$$n(FF_m) = \sum_y (FP_m)_y \quad (3)$$

where $n(FF_m)$ is the flood frequency for month, $m = (FP_m)_y$ is flood pixel for the month for corresponding year ($y = \text{year i.e. } 2015, 2016, \dots, 2018$) ($m = \text{month i.e. February, } \dots, \text{September}$)

Results and discussion

In this section, LULC, accuracy assessment and spatial extent of flooded areas have been generated for each district. In addition, we identified the flood frequency in each month of the *belg* and *meher* seasons. This study identified 29 administrative units affected by floodwaters.

Spatial distribution of land use/land cover

Figure 4 illustrates the spatial distribution of LULC during 2017 period for Awash basins that feed into the Afar region. The generated LULC map consisted of eight classes i.e., barren land/wasteland, grassland, rainfed-single crop (SC)-croplands,

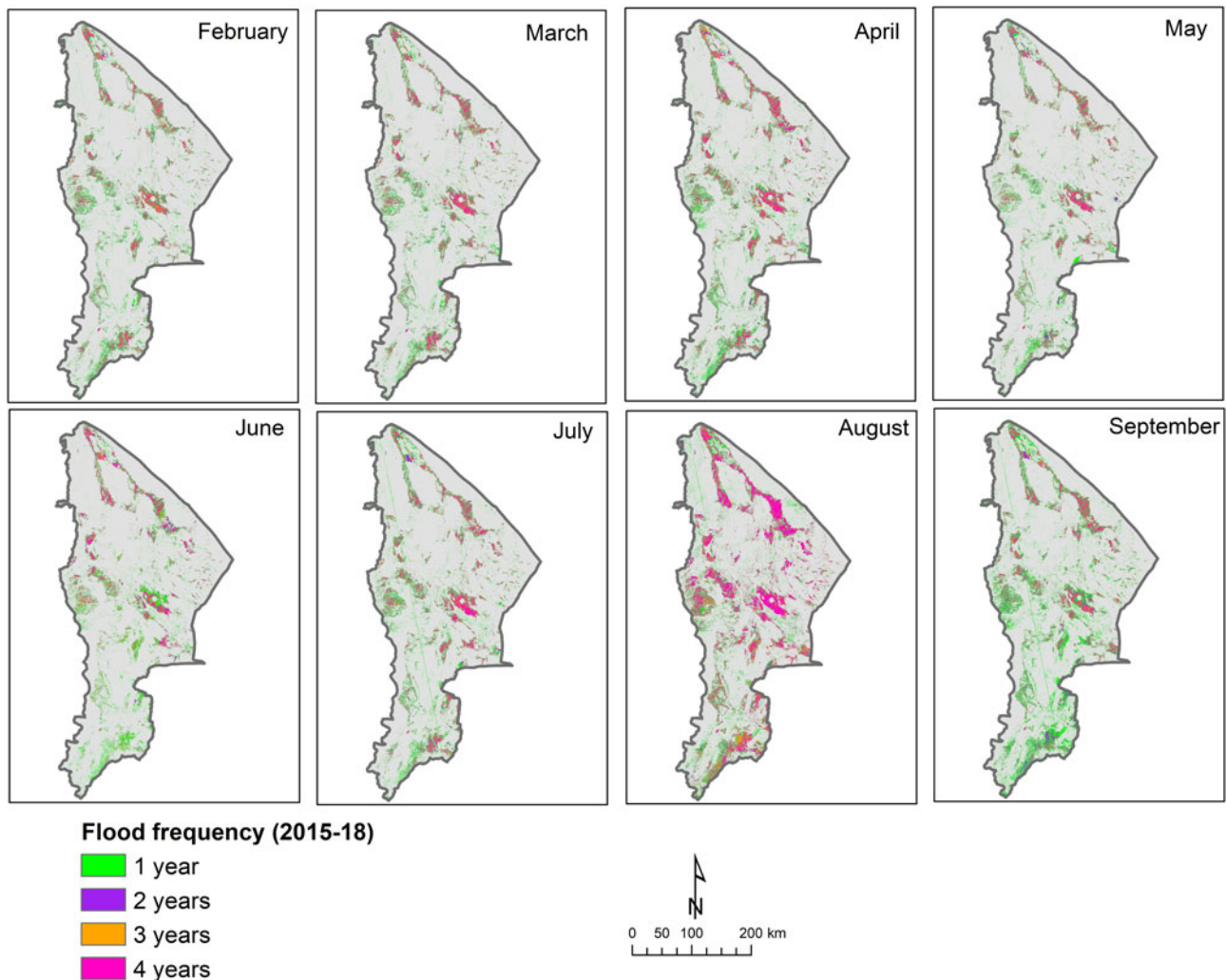


Fig. 6. Temporal changes in flooded area in the Afar region.

irrigated-SC-croplands, irrigated-double crop (DC)-croplands, forest/shrub lands/grasslands, built up lands and water bodies. About 85% of total area currently accounts for non-agricultural land. The majority of LULC comprises barren land/wasteland, forest/shrub lands/grasslands etc. Built-uplands and waterbodies covered the least area i.e. 79,462 and 83,013 ha, respectively (Table 2). Rainfed agriculture covers 1,275,443 ha whereas irrigated single and double croplands cover 1,451,694 ha.

Accuracy assessment

A quantitative accuracy assessment was done through an error matrix (Jensen, 1996) to examine LULC units. The ground survey data was based on an extensive field campaign conducted throughout the Afar region during the *meher* seasons for the crop years of 2016–2017. Accuracy was performed on classified LULC 2016–2017 map. The remaining 363 ground data points were used as validation to assess LULC classification accuracy. Accuracy assessment was performed with independent datasets.

Table 3 shows the error matrix of each product. In LULC, considering non-agricultural classes (1, 2, 6, 7 and 8) out of 170 points 149 points are correct with nearby user's accuracy of 88%. For an agricultural class like rainfed-SC-croplands (cl_04)

out of 22 points 16 were correct, while for irrigated-SC-croplands (cl_05) out of 10 points 10 were correct, while for irrigated-DC-croplands-croplands (cl_06) out of 35 points 27 were correct. Considering the overall agricultural classes, 53 out of 67 points were correct with user's accuracy of 80%. For all the 11 classes, 213 points out of 248 matched with the same class of reference data. The accuracy for the final eight classes of 2017 was 85.89% with a κ value of 0.8277 (Table 3). The loss of accuracy was mainly due to the coarse resolution of MODIS data.

Spatial distribution of flooded areas

Table 4 provides the proportion of flooded area under various LULC, disaggregated by slope category. Barren land/wasteland and forest/shrub lands/grasslands LULC classes are found to be the most flood prone areas under each slope category. Areas with a slope less than 2% comprised the dominant flooded area in Afar. About 50,303, 13,130 and 66,909 ha of the cultivated (rainfed and irrigated) land under slope category of <2, 2–3 and >3%, respectively, were found to be flood prone areas. The spatial distribution and extent of flooded area varied from month to month and from year to year (Figs. 5a and 5b).

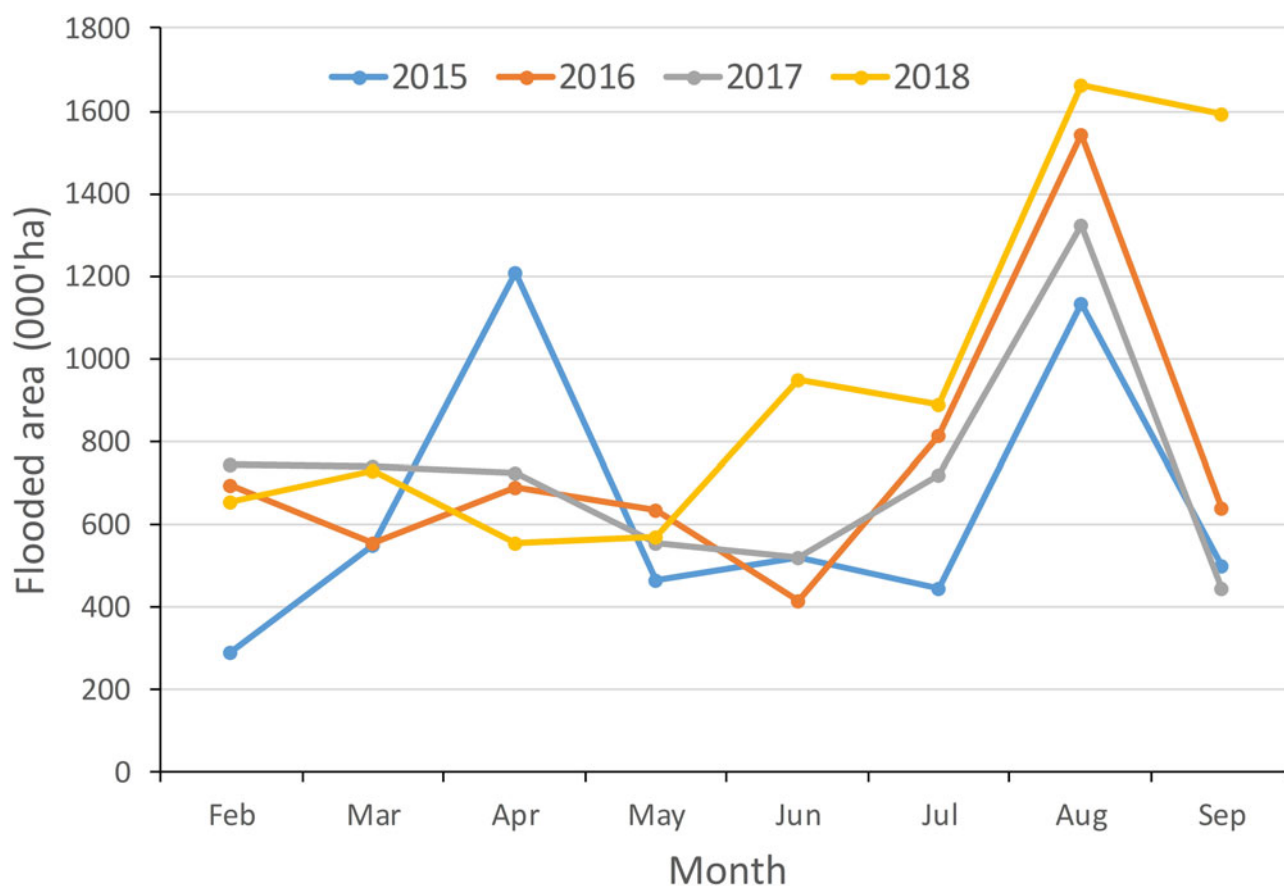


Fig. 7. Identification of flood prone areas and number of years in which flood occurred between 2015 to 2018.

Table 6. Area of land in ha and percentage of the total area in Afar that received flood corresponding to various frequencies (the number of years of occurrence within 4 years) between 2015 and 2018

Flood frequency	Area in '000 ha (%)							
	Feb	Mar	Apr	May	Jun	Jul	Aug	Sep
1 year	573 (6.1)	571 (6.1)	672 (7.1)	548 (5.8)	586 (6.2)	632 (6.7)	713 (7.6)	1038 (11)
2 years	347 (3.7)	342(3.6)	401 (4.3)	327 (3.5)	240 (2.5)	369 (3.9)	459 (4.9)	454 (4.8)
3 years	237 (2.5)	242 (2.6)	301 (3.2)	204 (2.2)	217 (2.3)	269 (2.9)	463 (4.9)	249 (2.6)
4 years	102 (1.1)	148 (1.6)	200 (2.1)	103 (1.1)	172 (1.8)	172 (1.8)	658 (7)	121 (1.3)

Temporal variation of flood in Afar

In all years but 2015, the flooded areas during the *meher* season were larger than the area flooded during the *belg* season. Ground observations also showed that the year 2015 received uniquely high *belg* floods and lower *meher* flood events compared with a 'normal' year. In 2015, the July flood covered the smallest area of about 443,000 ha compared to the 815,000 ha in 2016; 720,000 ha in 2017 and 887,000 ha in 2018 (Fig. 5b). July is a critical month for flood-based production system due to the fact that planting depends mainly on the flood received during this month. August is a month with a large area of flood across years as it is the peak rainy month in the upstream highlands. Regular flooding in July may allow more successful implementation of feed and food

production because flood would continue to occur in the succeeding month of August, with higher confidence. Generally, a minimum of 720,000 and 550,000 ha of land could be considered for planning flood-based development in Afar using the *meher* and *belg* seasons, respectively. The actual amount of land that could be developed each season could, however, be less than the identified area due to poor soils and very high temperature in the eastern part of the basin. The socio-economic conditions, particularly the pastoral settings of the community, may not also allow farming in some grids even if flood is available. Table 5 and Figure 6 show temporal variations of flooded areas across the study region. Figure 6 clearly shows that flooding was less in 2015 compared with the other years.

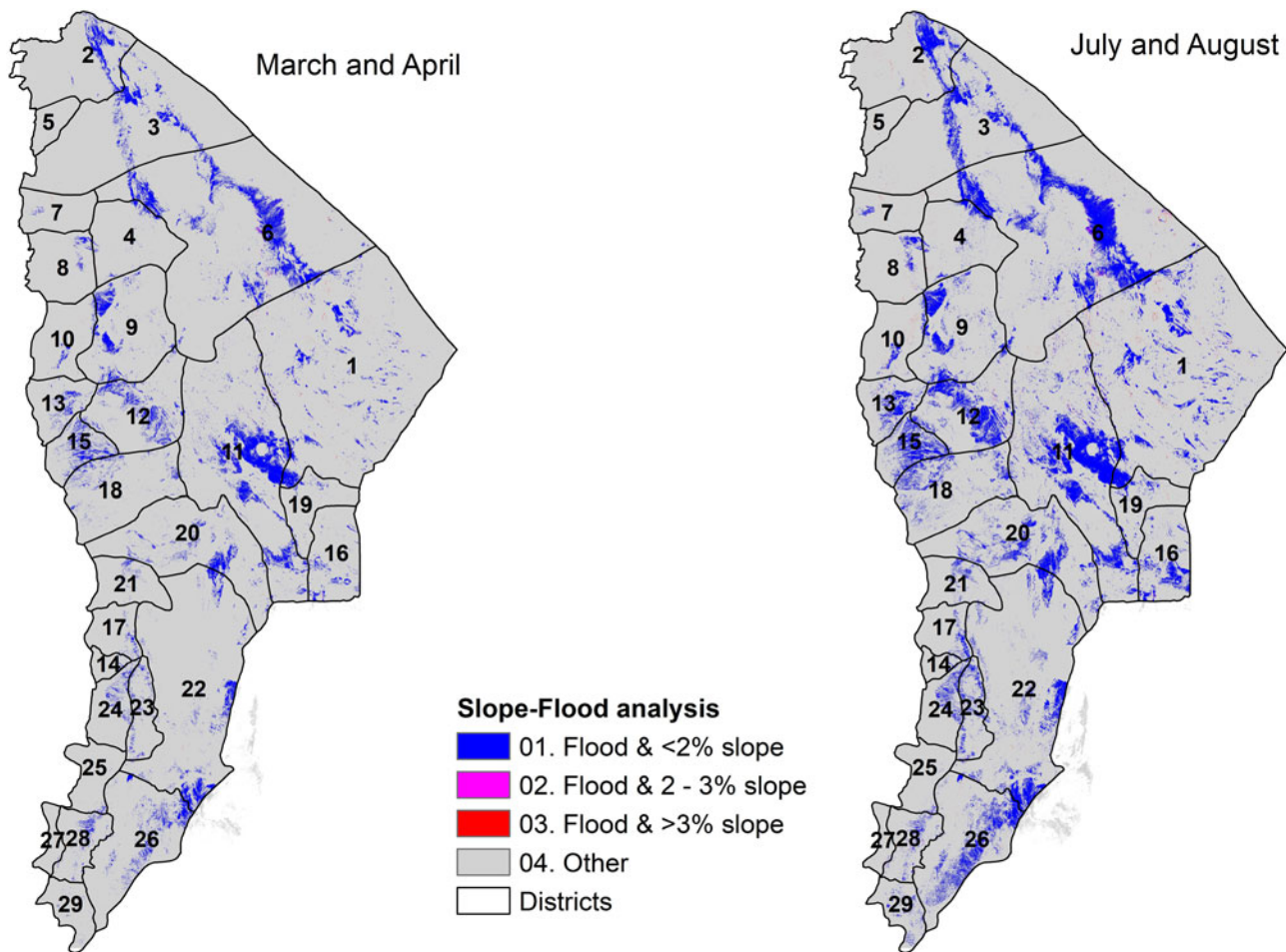


Fig. 8. Spatial distribution of flooded area in slope categories.

Flood frequency and distribution during the belg and meher seasons

Flood frequency was determined as the number of months and years a certain grid receives out of the 4 years of the study period (Fig. 7). Consequently, March and April covered a larger area with the highest frequency of flood during the *belg* season whereas July and August covered a larger area with the highest frequency of flood events for the *meher* seasons. Areas with the highest flood frequency have the lowest risk of water scarcity for productive use across years.

A minimum of 148,000 and 172,000 ha of land received flood in four out of the 4 years, between 2015 and 2018 for *belg* and *meher* seasons, respectively (Table 6). With a 75% chance of occurrence (three out of 4 years), the flooded area for *belg* and *meher* seasons could increase up to 242,000 and 463,000 ha, respectively. The highest the chance of getting flood every year, the lowest the area that can be flooded and vice versa. Therefore, the selection of areas for flood-based farming could be prioritized using the flood frequency across years with the premises that ‘the highest the frequency, the higher the priority’.

Flood maps

In order to ensure sustainable production, the reduce effect of floods and minimize drought risks in these drought-prone

systems, the most prospective strategy appears to partially harvest the available runoff for irrigating crops and rangelands (Sharma *et al.*, 2006). The horrendous flood emerging from the highlands could be partly converted to productive use (Amede *et al.*, 2009). Our research showed that these dry lowlands, which are commonly neighboring with upstream highlands receiving high rainfall amounts (>1000 mm per year) could be reliable sources of floodwaters. Furthermore, the adjacent highlands are characterized by the high frequency of intense rainfall with good flood potential compared with the lowland that receives only a few events with high intensity rainfall. Our analysis on rainfall data (1980–2010) for Chifra area and adjacent highlands depict that the lowland experienced on average 11 days of rainfall events with greater than 10 mm per day whereas the adjacent highland crossed this threshold in 32 days per year (<https://public.wmo.int/en/members/ethiopia>). For the higher intensity of at least 20 mm per day, the lowland receives only 2 days per year on average whereas the highland receives in 12 days per year. These demonstrate that the flood that could be available in the lowlands is a function of climate characteristics in the adjacent highlands. Therefore, the minimum area that is determined to be available for flood-based development could be affected by climate variability upstream.

Given the fact that the region is commonly inhabited by pastoral communities, the identification of potential areas should be developed in consultation with the local residents, who are

Table 7. Areas prone to flooded, per district, for three categories of drought frequency *belg* and *meher* season (during 2015–2018)

Unique ID	District	Area (ha)							
		<i>belg</i> season				<i>meher</i> season			
		01. Flood & <2% slope	02. Flood & 2–3% slope	03. Flood & >3% slope	04. Other	01. Flood & <2% slope	02. Flood & 2–3% slope	03. Flood & >3% slope	04. Other
1	ELIDAR	54,507	1223	1253	1,326,650	103,028	2647	3061	1,274,908
2	DALLOL	22,565	19	21	312,962	35,867	57	828	298,816
3	BERAHLE	31,147	10	76	703,157	52,936	99	421	680,934
4	EREBTI	5453	54	50	240,118	11,908	145	249	233,374
5	KONEBA	1	0	2	67,537	30	7	45	67,458
6	AFDERA	118,546	1691	393	1,216,412	199,242	3650	1467	1,132,683
7	ABALA	606	16	57	127,358	1916	58	255	125,809
8	MEGALE	3744	138	34	192,863	7342	282	202	188,953
9	TERU	27,667	270	44	337,758	44,045	529	198	320,967
10	YALO	4223	35	92	177,635	8355	153	572	172,904
11	DUBTI	109,308	1005	380	758,533	166,118	2590	1238	699,281
12	HABRU	29,213	191	94	271,968	65,802	693	374	234,596
13	GULINA	7098	82	15	125,357	18,866	358	117	113,211
14	ARTUMA	726	7	0	36,681	1080	9	3	36,322
15	EWA	18,023	104	1	102,366	36,049	155	4	84,285
16	AFAMBO	8833	133	60	215,409	25,336	196	73	198,830
17	DEWE	2811	2	0	103,153	6137	11	7	99,812
18	CHIFRA	11,449	53	19	317,587	32,184	167	27	296,729
19	AYSAITA	3429	10	38	136,592	8119	39	126	131,785
20	MILLE	23,196	100	78	457,435	52,697	246	86	427,779
21	TELALAK	2665	9	1	136,425	6384	41	5	132,670
22	GEWANE	39,985	120	95	824,990	76,624	514	168	787,884
23	BURE_MUDAY	5793	46	0	111,939	14,220	88	0	103,470
24	FURSI	6973	48	1	121,333	13,170	76	8	115,100
25	SIMUROBI_G	976	35	5	123,722	1043	37	26	123,632
26	AMIBARA	25,525	130	50	367,300	63,081	417	195	329,312
27	ARGOBA_SPE	163	22	13	46,898	254	42	56	46,743
28	DULECHA	6330	226	13	120,101	7824	394	35	118,417
29	AWASH_FENT	748	7	2	101,291	5176	97	30	96,746
	Total area	571,705	5784	2888	9,181,528	1,064,834	13,798	9877	8,673,407

commonly implementing pastoral based and mobile livelihood strategies and considering socio-economic, agro-ecological and technical aspects (Seid *et al.*, 2016). Therefore, once flood is received downstream, there is a huge opportunity to use it for food and feed production while at the same time rehabilitating degraded range lands (ICRISAT, 2017). Similar works have also demonstrated the use of flood for crop production (Tesfai and Stroosnijder, 2001; Tesfai and Sterk, 2002; Ham, 2008; Steenbergen *et al.*, 2011). However, the utilization should not be limited to forage and crop production. Construction of reservoirs or alternative water storage tanks may allow (agro)pastoralists

have access to livestock drinking water during extended dry periods. However, the feasibility of such alternatives needs to be understood in advance.

The month of April in the *belg* season and the month of August in the *meher* season are the periods that have larger area coverage of higher frequency flood (Fig. 8). In the Afar region, both seasons show an increase of intensity of flood from *belg* season to *meher* season. The majority of flood is under the slope of less than 2%. However, monthly flood distribution may not be the same from year to year following the climate variability in upstream highlands that are the major source of flood. The use

of water storage facilities could buffer the impact of climate variability on downstream flood availability. It could help to utilize the excess flood that may come from highlands during wet years for use in succeeding dry periods, which on the other hand may reduce the negative impacts of floods downstream.

The total areas of flood under three slope categories, which are <2, 2–3 and >3%, these areas increase from 571,705, 5,784 and 2,888 ha to 1,064,834, 13,798 and 9877 ha respectively from *belg* season to *meher* season. Almost all the districts in the Afar region are affected by floods. Afdera and Dupti districts have the largest coverage of flooded area in both seasons compared with other districts in Afar (Table 7), whereas Koneba district has less flooded area. The flooded area in Afdera increased from 118,546 to 199,242 ha from *belg* to *meher* season respectively whereas in Dubti it increased from 109,308 to 166,118 ha.

Practical implementation development programs using flood made available downstream in Afar requires consideration of additional factors. Some of the locations where flood is available may not be suitable for farming due to some limiting factors such as extreme salinity, very shallow rooting depth and scattered patches of flood areas that are too small to put long term investment. Moreover, feed and crop production should consider access to main roads and market hubs, willingness of the local government to invest on flood-based technology transfer and strong commitment of the local community. We further focus on how remote sensing technology will help in renewable food systems and also focus on climate change analysis for the future sustainable food security.

Conclusions

In this study, we categorized flood prone areas in the Afar region to target the dissemination of innovation technology for improving livelihoods, livestock and food production. First, we mapped land use land cover maps for study area into eight classes using Landsat-8 and MODIS temporal data for the year 2017. Accuracy assessment was performed based on ground survey data gave 86% of overall accuracy. Secondly, we extracted the slope map from SRTM DEM. Then, the slope maps were integrated with LULC and categorized slope wise LULC areas for the study region. Third, we mapped monthly flooded areas for *belg* and *meher* seasons. Further flood maps were integrated with temporal maps for each month and classified it into four classes. The maximum possible flooded areas were integrated with slope classes and generated maps along with statistics for the districts in the Afar region.

We have mapped the flood extent and database for 4 years (starting from 2015 to 2018) in the Afar region. The methodology was used to determine intensity of flood. Mapping flood prone areas are very important to understand Afar region and identifying locations for effective utilization. Up-to-date flood maps are an important input for decision making to improve natural resource management technologies. Therefore, we conclude that the method is suitable for identifying flood potential of regions or basins to guide strategic planning of flood-based development in Afar and similar areas.

Future research can be focused on identify suitable techniques to construct water harvesting structures by using hydrological models and topographical analysis through the construction of water harvesting structures appropriate river channels. Results conclude that the methods are recommended for the identification of large scale flood mapping. Identifying various flood

prone areas based on flood frequency could help implement sustainable agriculture and fodder development. The developed database, maps and statistics are very much useful for site specific decision on production and cost analysis.

Acknowledgement. This project is conducted with the financial support and facilitation of GIZ-SDR Ethiopia. The authors are thankful to all the GIZ-SDR staff in Addis Ababa, Semera and Chifra and the Pastoral Agropastoral Development office (PADO) at Chifra and the local community at the project site for all support during the field work. This research was supported by the CGIAR Research Program Water, Land and Ecosystems (WLE) which is carried out with support from the CGIAR Trust Fund and through bilateral funding agreements. For details visit <https://wle.cgiar.org/donors>.

References

- Alsdorf DE, Rodríguez E and Lettenmaier DP (2007) Measuring surface water from space. *Reviews of Geophysics* **45**, 1–24.
- Amede T, Stroud A and Aune J (2004) Advancing human nutrition without degrading land resources through modeling cropping systems in the Ethiopian Highlands. *Food and Nutrition Bulletin* **25**, 344–353.
- Amede T, Descheemaeker K, Peden D and van Rooyen A (2009) Harnessing benefits from improved livestock water productivity in crop–livestock systems of sub-Saharan Africa: synthesis. *The Rangeland Journal* **31**, 169–178.
- Biggs TW, Thenkabail PS, Gumma MK, Scott CA, Parthasaradhi GR and Turrall HN (2006) Irrigated area mapping in heterogeneous landscapes with MODIS time series, ground truth and census data, Krishna Basin, India. *International Journal of Remote Sensing* **27**, 4245–4266.
- Cihlar J, Xiao Q, Chen J, Beaubien J, Fung K, Latifovic R (1998) Classification by progressive generalization: A new automated methodology for remote sensing multichannel data. *International Journal of Remote Sensing* **19**, 2685–2704.
- Dong J, Xiao X, Kou W, Qin Y, Zhang G, Li L, Jin C, Zhou Y, Wang J, Biradar C, Liu J and Moore B (2015) Tracking the dynamics of paddy rice planting area in 1986–2010 through time series Landsat images and phenology-based algorithms. *Remote Sensing of Environment* **160**, 99–113.
- Elisabeth V, Wolf B and Jemal NM (2015) Reversing natural degradation into resilience: the afar case. In Tielke E (ed.), *Management of Land use Systems for Enhanced Food Security: Conflicts, Controversies and Resolutions*. Berlin and Münchenberg: Cuvillier Verlag, p. 1. Available at www.tropentag.de/2015/proceedings/proceedings.pdf (Accessed 15 March 2019).
- Feyisa GL, Meilby H, Fensholt R and Proud SR (2014) Automated Water Extraction Index: a new technique for surface water mapping using Landsat imagery. *Remote Sensing of Environment* **140**, 23–35.
- Flick RE, Chadwick DB, Briscoe J and Harper KC (2012) Flooding” versus “inundation. *Eos, Transactions American Geophysical Union* **93**, 365–366.
- Giustarini L, Hostache R, Matgen P, Schumann GJ-P, Bates PD and Mason DC (2013) A change detection approach to flood mapping in urban areas using TerraSAR-X. *IEEE transactions on Geoscience and Remote Sensing* **51**, 2417–2430.
- Gumma M, Thenkabail PS, Fujii H and Namara R (2009) Spatial models for selecting the most suitable areas of rice cultivation in the Inland Valley Wetlands of Ghana using remote sensing and geographic information systems. *Journal of Applied Remote Sensing* **3**, 033537. P (1–21).
- Gumma MK, Thenkabail PS, Muralikrishna IV, Velpuri MN, Gangadhararao PT, Dheeravath V, Biradar CM, Acharya Nalan S and Gaur A (2011) Changes in agricultural cropland areas between a water-surplus year and a water-deficit year impacting food security, determined using MODIS 250 m time-series data and spectral matching techniques, in the Krishna River basin (India). *International Journal of Remote Sensing* **32**, 3495–3520.
- Gumma MK, Thenkabail PS, Maunahan A, Islam S and Nelson A (2014) Mapping seasonal rice cropland extent and area in the high cropping intensity environment of Bangladesh using MODIS 500 m data for the year 2010. *ISPRS Journal of Photogrammetry and Remote Sensing* **91**, 98–113.

- Gumma MK, Uppala D, Mohammed IA, Whitbread AM and Mohammed IR** (2015) Mapping direct seeded rice in Raichur District of Karnataka, India. *Photogrammetric Engineering & Remote Sensing* **81**, 873–880.
- Gumma M, Birhanu B, Mohammed I, Tabo R and Whitbread A** (2016) Prioritization of watersheds across Mali using remote sensing data and GIS techniques for agricultural development planning. *Water* **8**, 260.
- Gumma MK, Mohammad I, Nedumaran S, Whitbread A and Lagerkvist C** (2017) Urban sprawl and adverse impacts on agricultural land: a Case Study on Hyderabad, India. *Remote Sensing* **9**, 1136.
- Gumma MK, Thenkabail PS, Deevi KC, Mohammed IA, Teluguntla P, Oliphant A, Xiong J, Aye T and Whitbread AM** (2018a) Mapping cropland fallow areas in Myanmar to scale up sustainable intensification of pulse crops in the farming system. *GIScience & Remote Sensing* **55**, 926–949.
- Gumma MK, Thenkabail PS, Teluguntla P and Whitbread AM** (2018b) Monitoring of spatiotemporal dynamics of rabi rice fallows in south Asia using remote sensing. In Reddy G and Singh S (eds), *Geospatial Technologies in Land Resources Mapping, Monitoring and Management*. Vol. 21, Cham: Springer, pp. 425–449.
- Gumma MK, Nelson A and Yamano T** (2019) Mapping drought-induced changes in rice area in India. *International Journal of Remote Sensing* **40**, 8146–8173.
- Gummadi S, Rao KPC, Seid J, Legesse G, Kadiyala MDM, Takele R, Amede T and Whitbread A** (2017) Spatio-temporal variability and trends of precipitation and extreme rainfall events in Ethiopia in 1980–2010. *Theoretical and Applied Climatology* **134**, 1315–1328.
- Haile G and Fetene M** (2012) Assessment of soil erosion hazard in Kilie catchment, East Shoa, Ethiopia. *Land Degradation & Development* **23**, 293–306.
- Hailu R, Tolossa D and Alemu G** (2018) Water institutions in the Awash basin of Ethiopia: the discrepancies between rhetoric and realities. *International journal of river basin management* **16**, 107–121.
- Ham J-PVD** (2008) Dodota Spate Irrigation System Ethiopia: A case study of Spate Irrigation Management and Livelihood options. Irrigation and Water Engineering. Wageningen University and Research, Wageningen University and Research.
- Hurni H** (1988) Degradation and conservation of the resources in the Ethiopian highlands. *Mountain Research and Development* **8**, 123–130.
- ICRISAT** (2017) The lone green patch on a denuded stretch-cCase of the Afar region in Ethiopia. ICRISAT Happening No. 1742.
- Iqbal M and Sajjad H** (2014) Prioritization based on morphometric analysis if Dudhganga catchment, Kashmir valley, Inida, using remote sensing and geographical information system. *African Journal of Geo-Sciences Research* **2**, 01–06.
- Jensen JR** (1996) *Introductory Digital Image Processing: A Remote Sensing Perspective*. Upper Saddle River, New Jersey: Prentice Hall.
- Jung HC, Hamski J, Durand M, Alsdorf D, Hossain F, Lee H, Hossain AA, Hasan K, Khan AS and Hoque AZ** (2010) Characterization of complex fluvial systems using remote sensing of spatial and temporal water level variations in the Amazon, Congo, and Brahmaputra Rivers. *Earth Surface Processes and Landforms: The Journal of the British Geomorphological Research Group* **35**, 294–304.
- Khan M, Gupta V and Moharana P** (2001) Watershed prioritization using remote sensing and geographical information system: a case study from Guhiya, India. *Journal of Arid Environments* **49**, 465–475.
- McCann JC** (1997) The plow and the forest: narratives of deforestation in Ethiopia, 1840–1992. *Environmental History* **2**, 138–159.
- Miheretu BA and Yimer AA** (2018) Estimating soil loss for sustainable land management planning at the Gelana sub-watershed, northern highlands of Ethiopia. *International Journal of River Basin Management* **16**, 41–50.
- Moore ID, Grayson R and Ladson A** (1991) Digital terrain modelling: a review of hydrological, geomorphological, and biological applications. *Hydrological Processes* **5**, 3–30.
- Paloscia S, Pettinato S, Santi E, Notarnicola C, Pasolli L and Reppucci A** (2013) Soil moisture mapping using sentinel-1 images: algorithm and preliminary validation. *Remote Sensing of Environment* **134**, 234–248.
- Panwar A and Singh D** (2014) Watershed development prioritization by applying WERM model and GIS techniques in takoli watershed of district Tehri (Uttarakhand). *International Journal of Engineering Research and Technology* **3**, 1597–1601.
- Pierdicca N, Pulvirenti L and Pace G** (2014) A prototype software package to retrieve soil moisture from sentinel-1 data by using a Bayesian multitemporal algorithm. *IEEE Journal of Selected Topics in Applied Earth Observations and Remote Sensing* **7**, 153–166.
- Qiu B, Zeng C, Tang Z and Chen C** (2013) Characterizing spatiotemporal non-stationarity in vegetation dynamics in China using MODIS EVI dataset. *Environmental Monitoring and Assessment* **185**, 9019–9035.
- Qiu B, Li W, Tang Z, Chen C and Qi W** (2015) Mapping paddy rice areas based on vegetation phenology and surface moisture conditions. *Ecological Indicators* **56**, 79–86.
- Rao NS, Chakradhar GK and Srinivas V** (2001) Identification of groundwater potential zones using remote sensing techniques in and around Guntur Town, Andhra Pradesh, India. *Journal of the Indian Society of Remote Sensing* **29**, 69.
- Schlaffer S, Matgen P, Hollaus M and Wagner W** (2015) Flood detection from multi-temporal SAR data using harmonic analysis and change detection. *International Journal of Applied Earth Observation and Geoinformation* **38**, 15–24.
- Seid N, Reda GK, Mohammed S, Bedru S, Ebrahim K, Teshale T and Demelash N** (2016) Socio-economic, Agro-ecological and Technical Potential of the Proposed Ascoma Spate Irrigation Project: Ada'ar Woreda, Afar National Regional State, Ethiopia. USAID, Feed the Future.
- Sharma R, Agrawal M and Marshall F** (2006) Heavy metal contamination in vegetables grown in wastewater irrigated areas of Varanasi, India. *Bulletin of environmental contamination and toxicology* **77**, 312–318.
- Steenbergen FV, Haile AM, Alemehayu T, Alamirew T and Geleta Y** (2011) Status and potential of spate irrigation in Ethiopia. *Water Resources Management* **25**, 1899–1913.
- Taddese G, Sonder K and Peden D** (2003) *The Water of the Awash River Basin A Future Challenge to Ethiopia*. Addis Ababa: International Livestock Research Institute.
- Tamene L and Vlek PL** (2008) Soil erosion studies in northern Ethiopia. In Braimoh AK and Vlek PLG (eds), *Land use and Soil Resources*. Dordrecht: Springer, pp. 73–100.
- Tesfai M and Stroosnijder L** (2001) The Eritrean spate irrigation system. *Agricultural Water Management* **48**, 51–60.
- Tesfai M and Sterk G** (2002) Sedimentation rate on spate irrigated fields in Sheeb area, eastern Eritrea. *Journal of Arid Environments* **50**, 191–203.
- Twele A, Cao W, Plank S and Martinis S** (2016) Sentinel-1-based flood mapping: a fully automated processing chain. *International Journal of Remote Sensing* **37**, 2990–3004.
- Van Steenbergen F, Haile AM, Alemehayu T, Alamirew T and Geleta Y** (2011) Status and potential of spate irrigation in Ethiopia. *Water Resources Management* **25**, 1899–1913.
- Vittala SS, Govindaiah S and Gowda HH** (2008) Prioritization of sub-watersheds for sustainable development and management of natural resources: an integrated approach using remote sensing, GIS and socio-economic data. *Current Science* **95**, 345–354.